Dissociation mechanism of lithium salt by BaTiO₃ with spontaneous polarization

Shaoke Guo[a,b,f], Shendong Tan[a,b,f], Jiabin Ma[a,b], Likun Chen[a,b], Ke Yang[a,b], Qiannan Zhu[a,b], Yuetao Ma[a,b], Peiran Shi[a,b], Yinping Wei[a,b], Xufei An[a,b], Qingkang Ren[c], Yanfei Huang[d], Yingman Zhu[a], Ye Cheng[a,b], Wei Lv[a], Tingzheng Hou[a]*, Ming Liu[a]*, Yan-Bing He[a]*, Quan-Hong Yang[e], Feiyu Kang[a,b]*

a Shenzhen All-Solid-State Lithium Battery Electrolyte Engineering Research Center, Institute of Materials Research (IMR), Tsinghua Shenzhen International Graduate School, Tsinghua University, Shenzhen 518055, China.

b. School of Materials Science and Engineering, Tsinghua University, Beijing, 100084, China.

c. College of Mechatronics and Control Engineering, Shenzhen University, Shenzhen, China.

d. College of Materials Science and Engineering, Shenzhen University, Shenzhen, China.

e. School of Chemical Engineering and Technology, Tianjin University, Tianjin 300072, P. R. China

f. These authors contributed equally: Shaoke Guo, Shendong Tan.

Correspondence and requests for materials should be addressed to Y.-B. H. (email: tingzhenghou@sz.tsinghua.edu.cn, liuming@sz.tsinghua.edu.cn, he.yanbing@sz.tsinghua.edu.cn, fykang@sz.tsinghua.edu.cn)
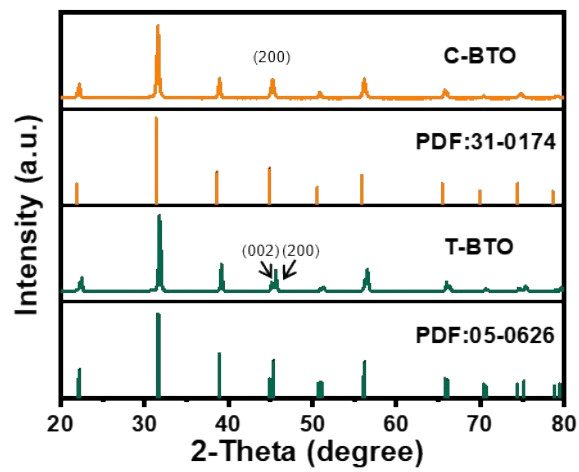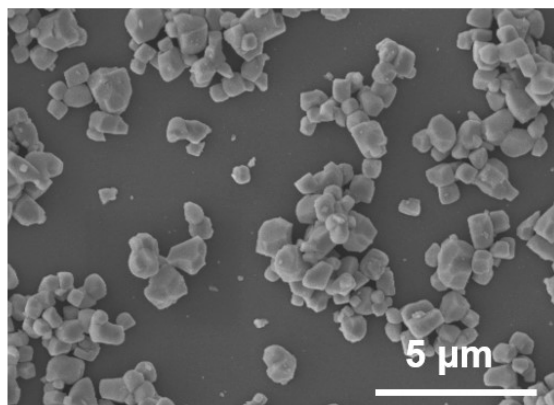
Supplementary Figures

Fig. S1 The XRD patterns of C-BTO and T-BTO.
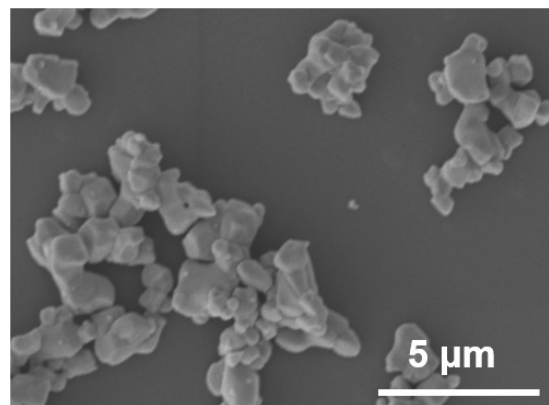
a

b

Fig. S2 Scanning electron microcopy (SEM) images of a) C-BTO and b) T-BTO particles.
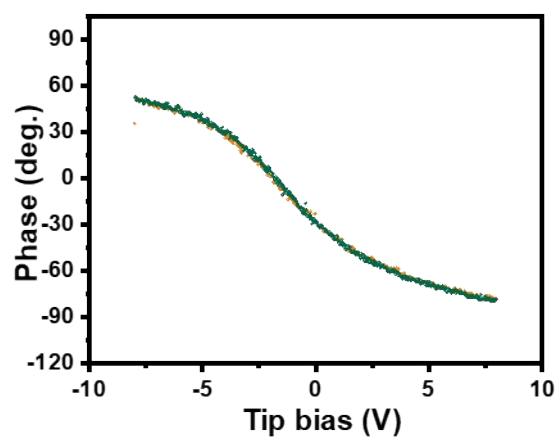
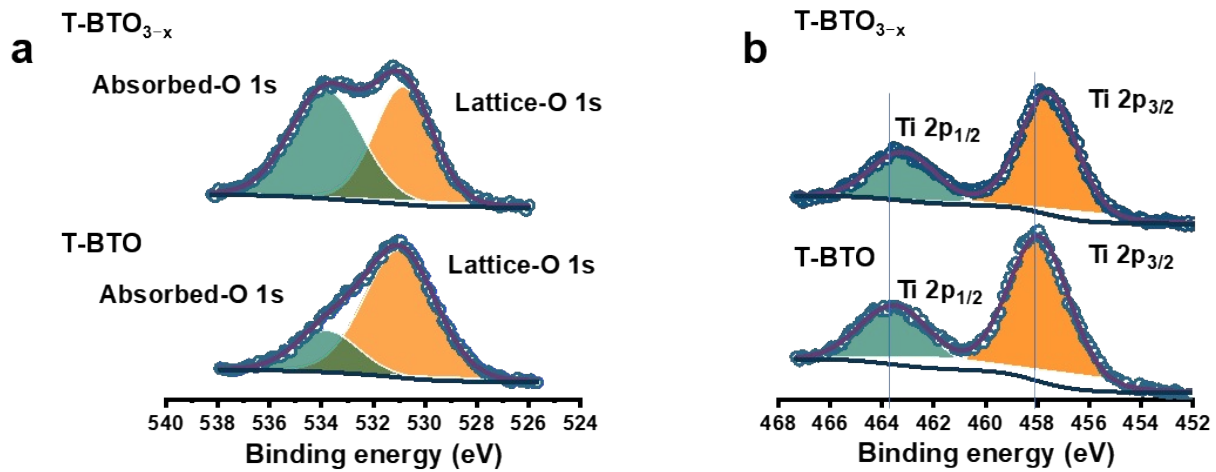**Fig. S3** Hysteresis loop of PVDF obtained from PFM analysis.

Fig. S4 The a) O 1s XPS spectroscopy of T-BTO and T-BTO$_{3-x}$ and b) Ti 2p$_{1/2}$ and 2p$_{3/2}$ XPS spectroscopy of T-BTO and T-BTO$_{3-x}$.
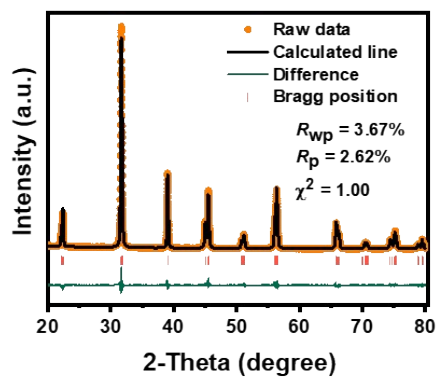
a

Intensity (a.u.)

Raw data
Calculated line
Difference
Bragg position

R_{wp} = 3.67%
R_p = 2.62%
χ^2 = 1.00

2-Theta (degree)

b

[001]

a
b
c

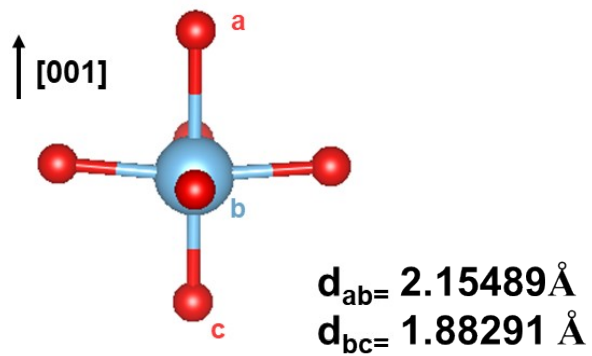d_{ab}= 2.15489Å
d_{bc}= 1.88291 Å

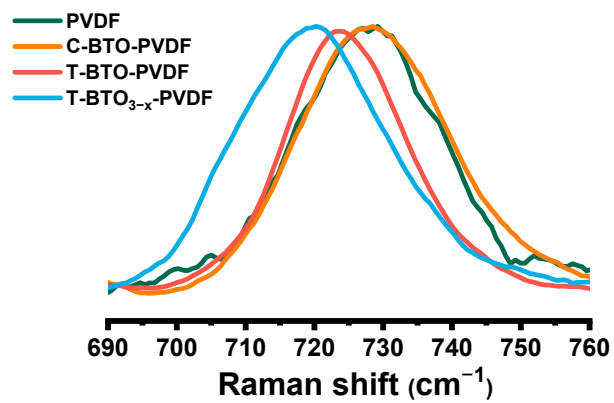**Fig. S5.** a) The XRD refinement of T-BTO and b) the illustration of Ti^{4+} deviation.

Fig. S6 Raman spectra of PVDF, C-BTO-PVDF, T-BTO-PVDF and T-BTO$_{3-x}$-PVDF.
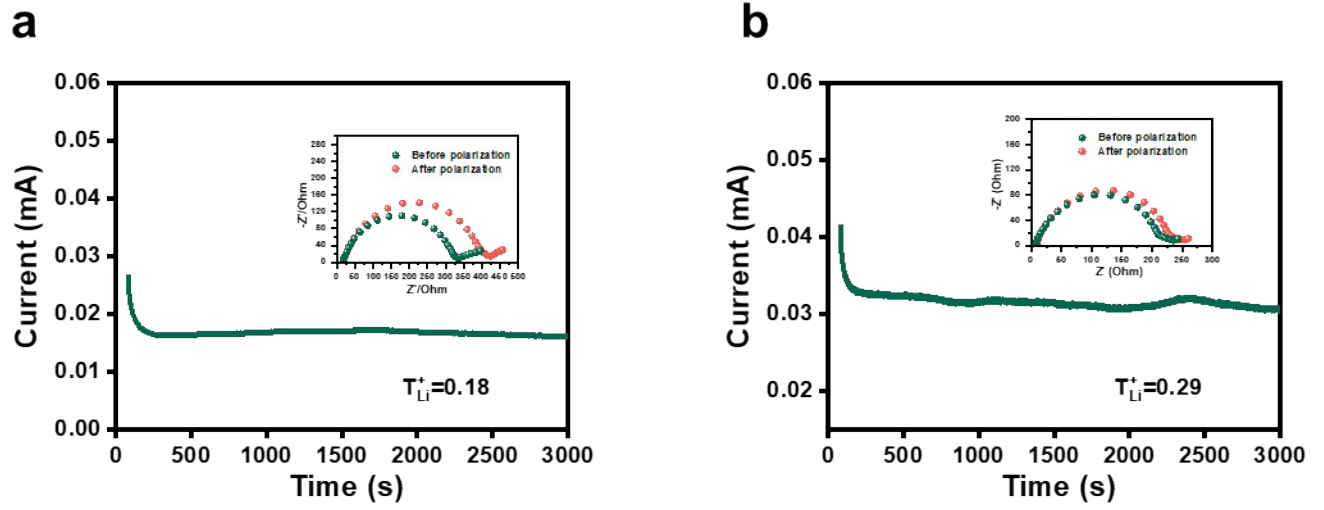
Fig. S7 Current-time profiles of Li‖Li symmetric batteries using a) PVDF and b) T-BTO-PVDF electrolytes.
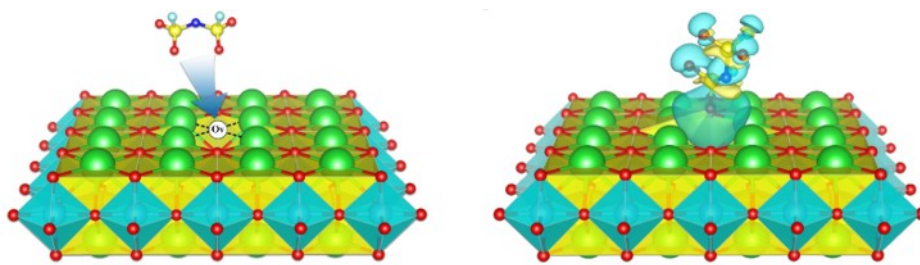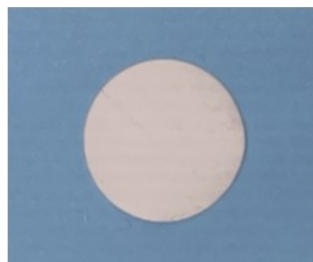
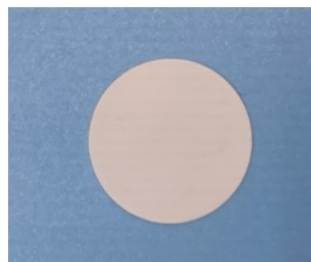**Fig. S8** Simulation of the OVs' adsorption effect on FSI⁻.

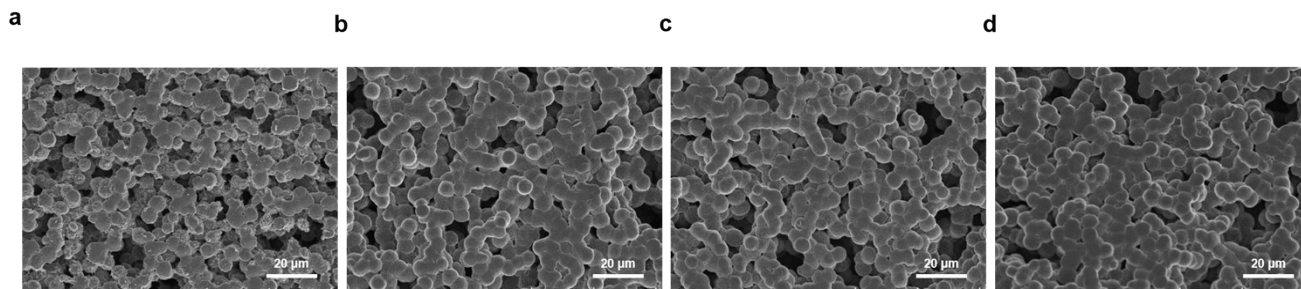**Fig. S9** Optical images of a) PVDF and b) T-BTO$_{3-x}$-PVDF electrolytes.

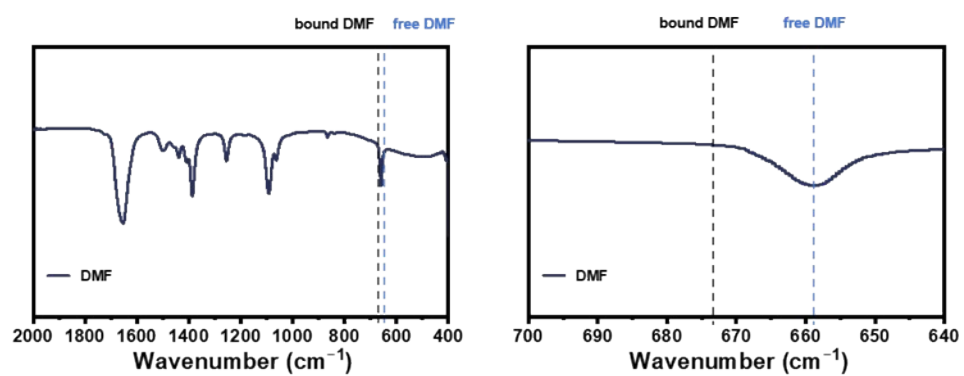**Fig. S10** The SEM images of the surface of a) PVDF, b) C-BTO-PVDF, c) T-BTO-PVDF and d) T-BTO$_{3-x}$-PVDF.

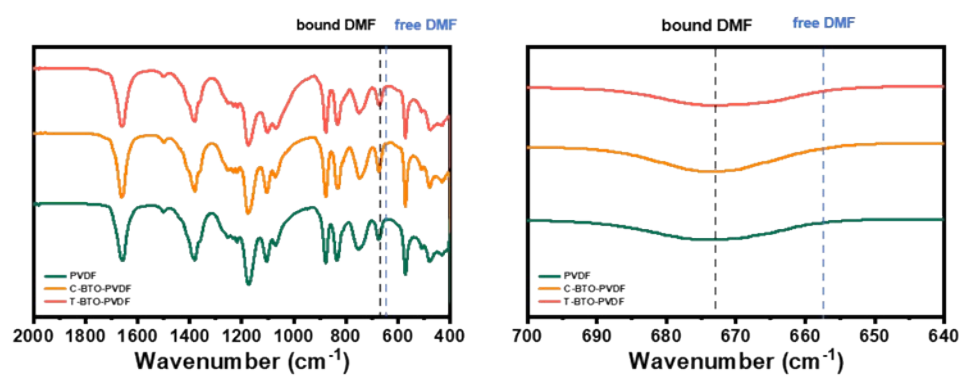**Fig. S11** FTIR spectra of DMF in the range of a) 400–2000 cm^{-1} and b) 640–700 cm^{-1}.

Fig. S12 FTIR spectra of DMF in PVDF-based electrolytes in the range of a) 400–2000 cm^{-1} and b) 640–700 cm^{-1}.
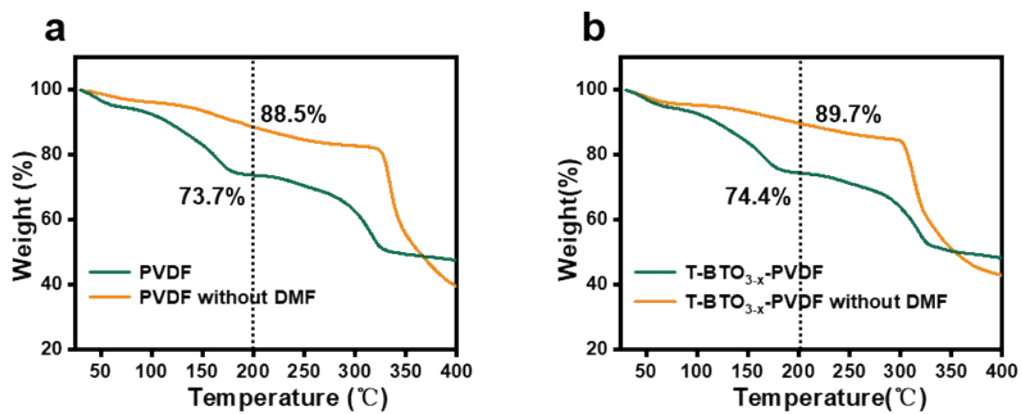
Fig. S13 TGA curves of a) PVDF, b) T-BTO$_{3-x}$-PVDF electrolytes and their samples without DMF at heating rate of 10 ºC min^{-1}.
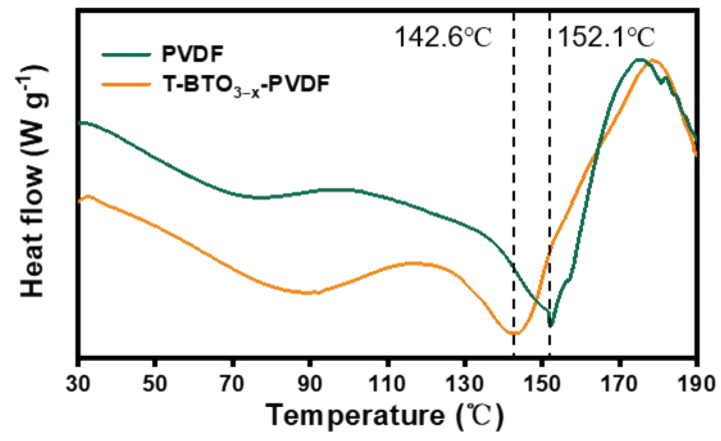
Fig. S14 DSC curves of PVDF and T-BTO$_{3-x}$-PVDF electrolyte.
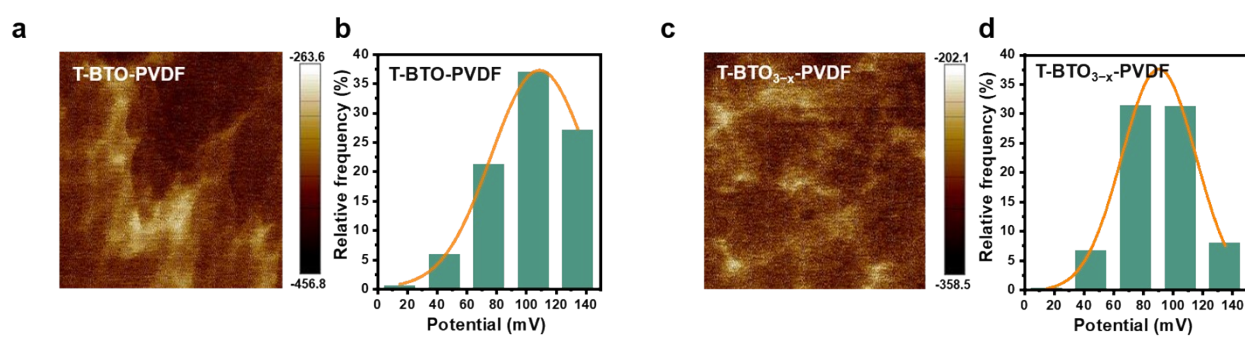
Fig. S15 Kelvin probe force microscopy interfacial potential images of the a) T-BTO-PVDF and c) T-BTO$_{3-x}$-PVDF electrolytes. Gauss statistic distribution histograms of the interfacial potential for b) T-BTO-PVDF and d) T-BTO$_{3-x}$-PVDF.
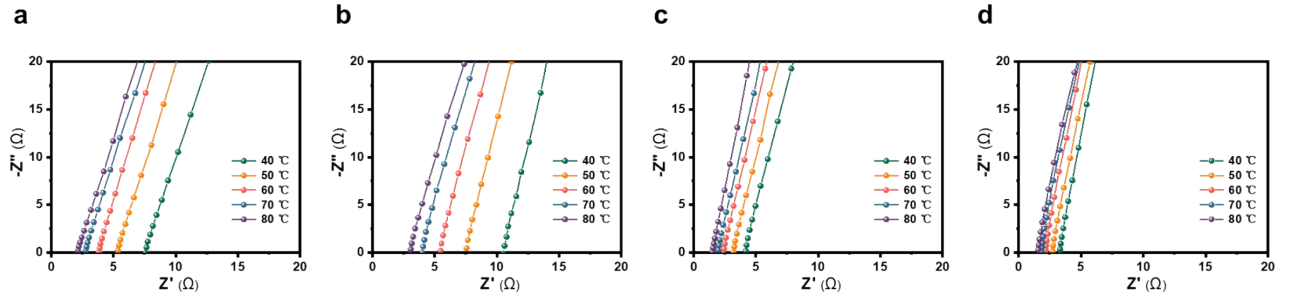
Fig. S16 Nyquist impedance spectra of stainless steel (SS)‖SS batteries with a) PVDF, b) C-BTO-PVDF, c) T-BTO-PVDF and d) T-BTO$_{3-x}$-PVDF at different temperatures.
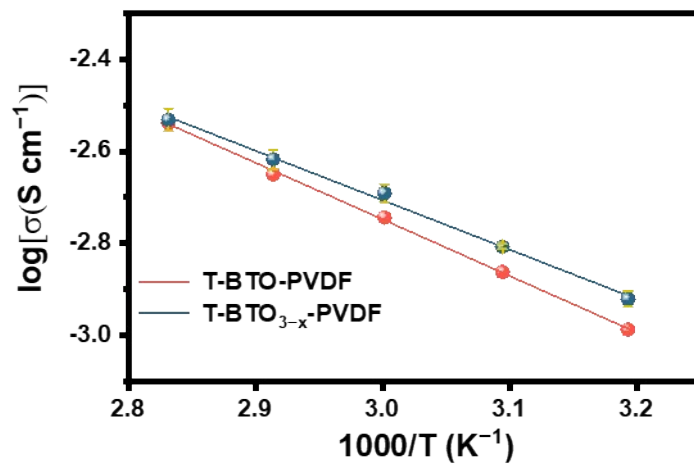
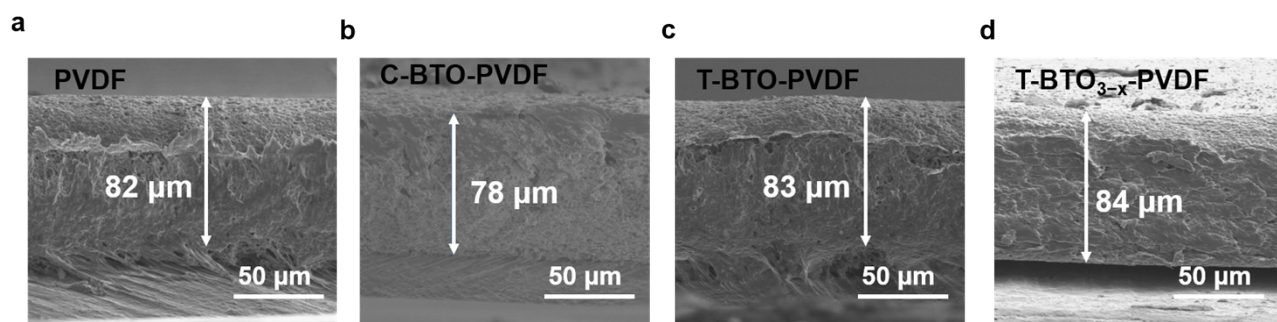**Fig. S17** Arrhenius plots of the T-BTO$_{3-x}$-PVDF electrolytes with error bar.

Fig. S18 Cross section SEM images of a) PVDF, b) C-BTO-PVDF, c) T-BTO-PVDF and d) T-BTO$_{3-x}$-PVDF.

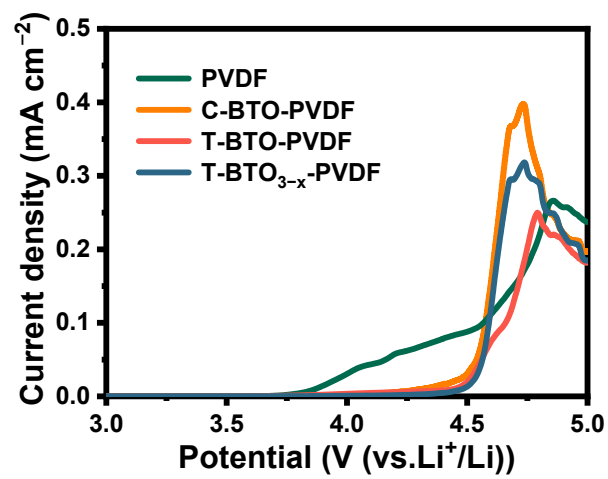**Fig. S19** LSV curves of SS‖Li batteries with different electrolytes.

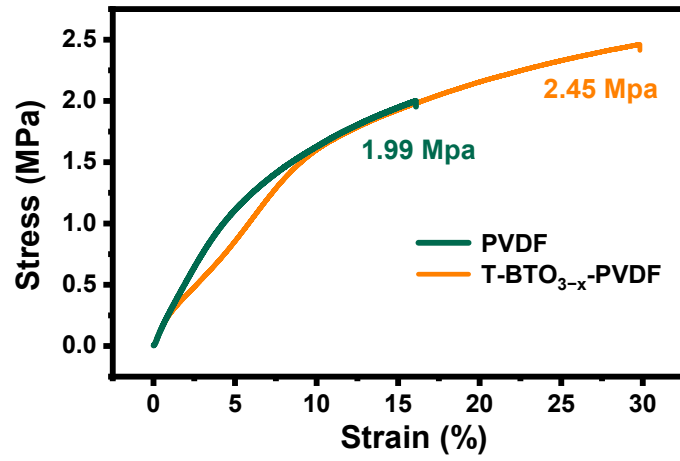**Fig. S20** Stress-strain curves of PVDF and T-BTO$_{3-x}$-PVDF electrolytes.
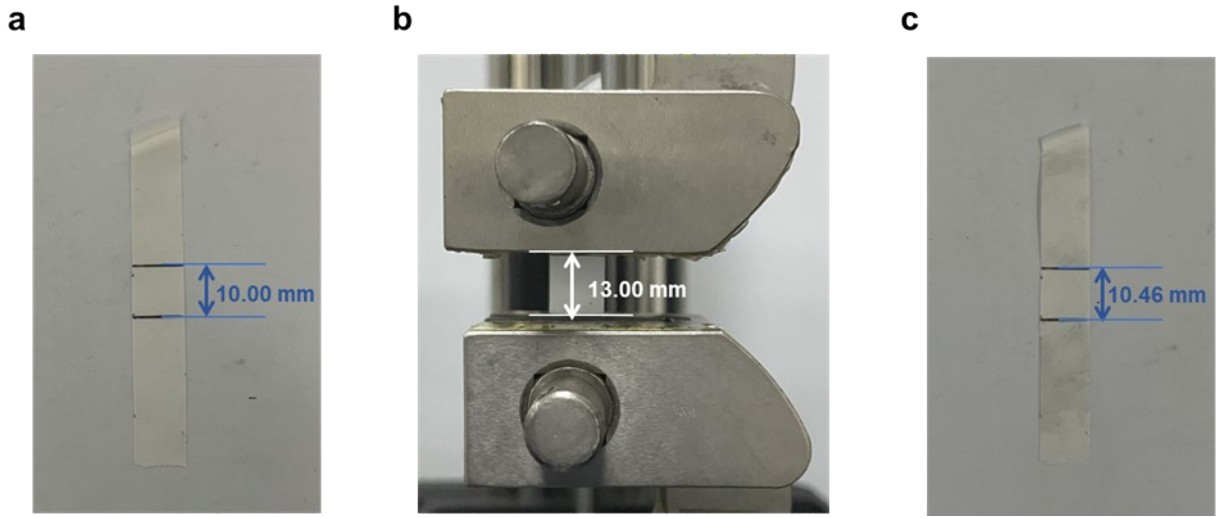
Fig. S21 The deformation state diagram of tensile test with T-BTO$_{3-x}$-PVDF electrolyte. a) The states before applying tensile force. b) The states of deformation with 30% strain. c) The states after applying tensile force.
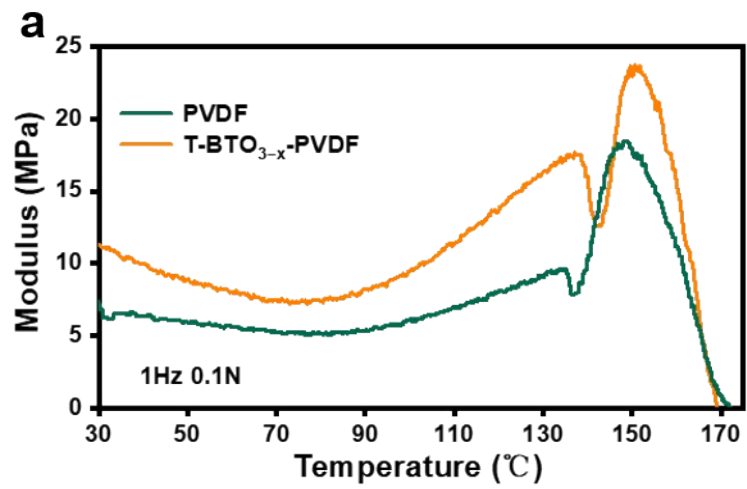
Fig. S22 Dynamic mechanical analysis (DMA) of PVDF and T-BTO$_{3-x}$-PVDF electrolytes at 1 Hz and 0.1 N.
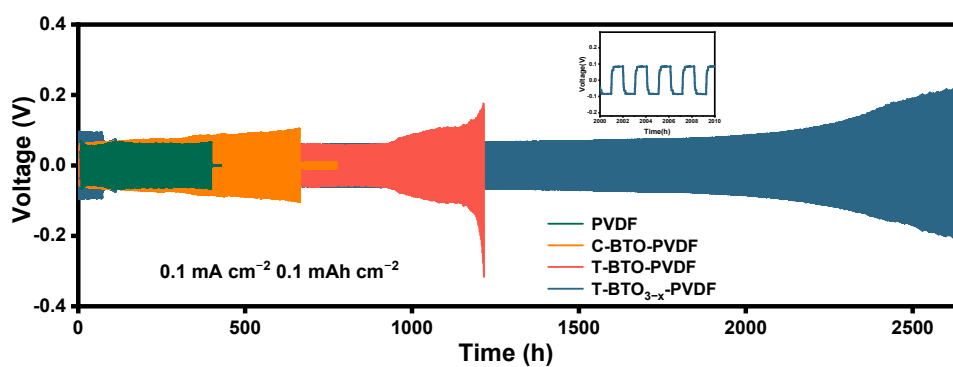
Fig. S23 Galvanostatic voltage profiles of Li||Li symmetric batteries at 0.1 mA cm^{-2} -0.1 mAh cm^{-2} with different electrolytes.

Fig. S24 a) Cross-sectional SEM images and EDS mappings of uncycled NCM811 cathode with loading of ~3 mg cm^{-2} contacted with PVDF electrolyte and EDS mappings of b) C, c) N, d) S, e) F and f) Al elements.
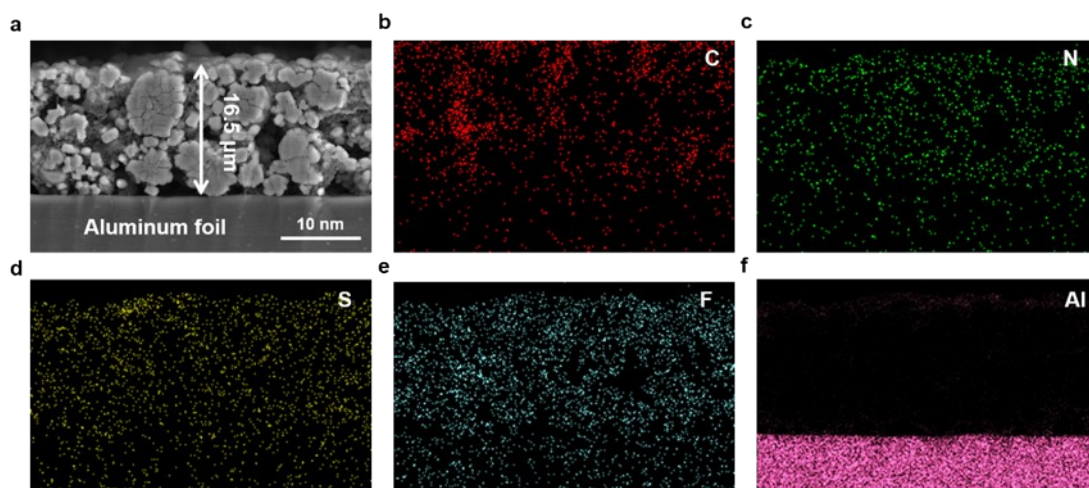
Fig.S25 a) Cross-sectional SEM images and EDS mappings of uncycled NCM811 cathode with loading of ~3 mg cm^{-2} contacted with T-BTO$_{3-x}$-PVDF electrolyte and EDS mappings of b) C, c) N, d) S, e) F and f) Al elements.

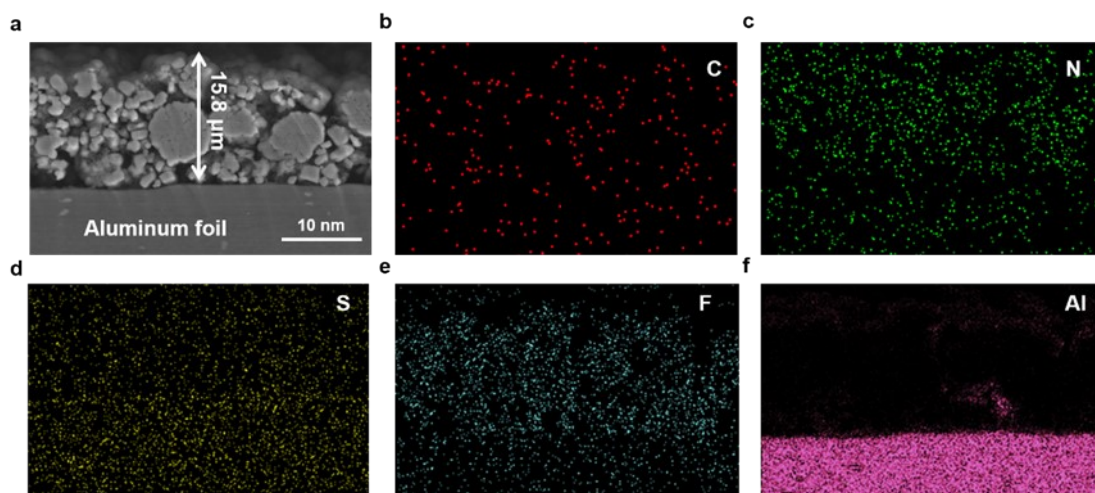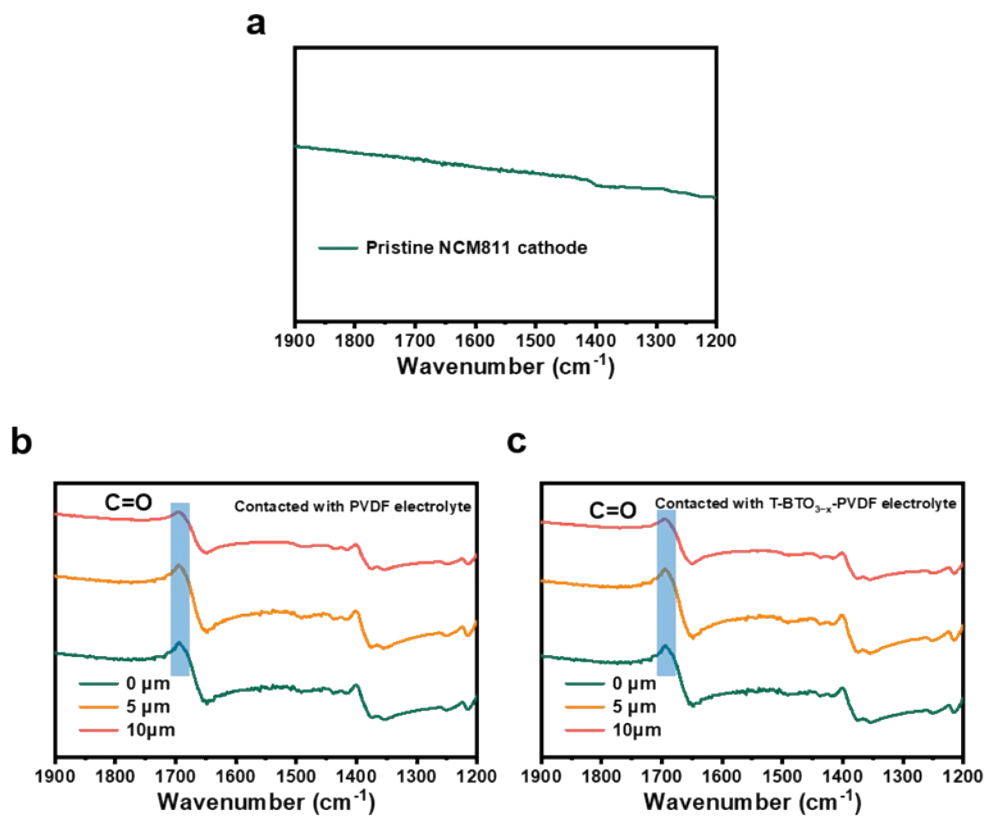**Fig. S26** FTIR spectra of a) pristine NCM811 cathode with loading of 3 mg cm^{-2}, contacted with b) PVDF and c) T-BTO$_{3-x}$-PVDF electrolyte.
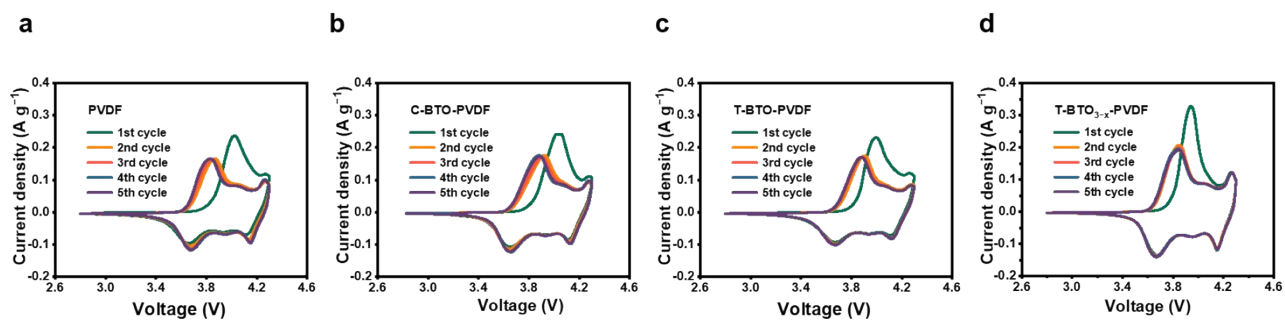
Fig.S27 Cyclic voltammogram (CV) curves of a) NMC811||PVDF||Li, b) NMC811||C-BTO-PVDF||Li, c) NMC811||T-BTO-PVDF||Li and d) NMC811||T-BTO$_{3-x}$-PVDF||Li.
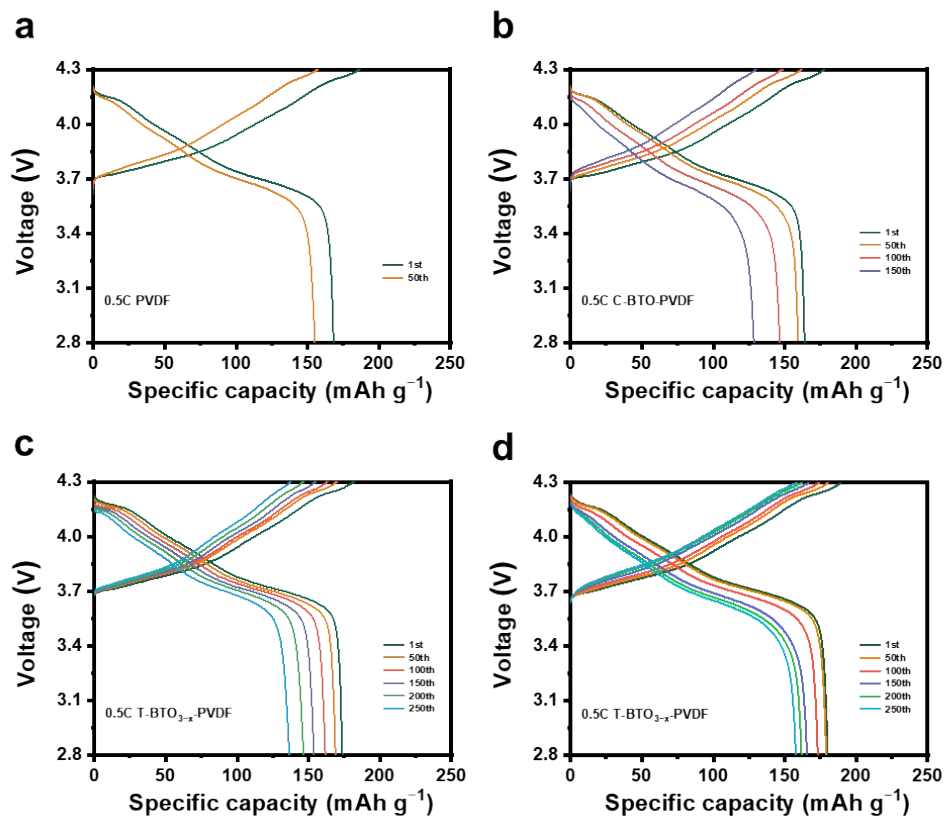
Fig. S28 Charge–discharge voltage profiles at 0.5 C with a) PVDF, b) C-BTO -PVDF, c) T-BTO -PVDF and d) T-BTO$_{3-x}$-PVDF.
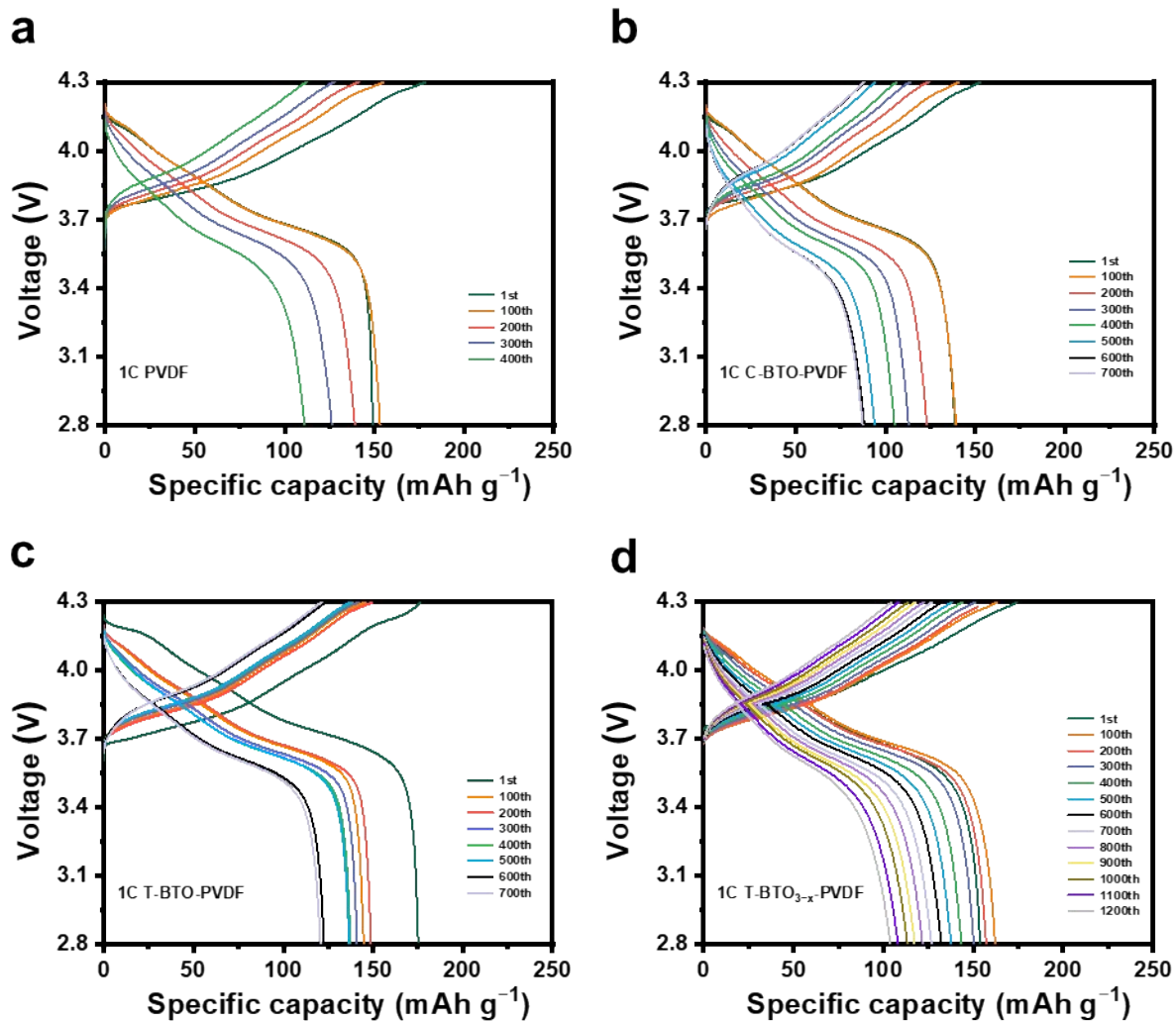
Fig. S29 Charge–discharge voltage profiles at 1 C with a) PVDF, b) C-BTO -PVDF, c) T-BTO - PVDF and d) T-BTO$_{3-x}$-PVDF.
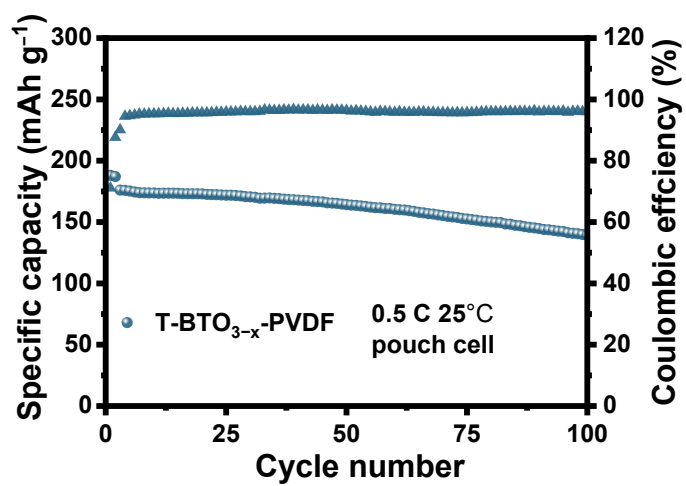
Fig. S30 Cycling performance of NCM811||T-BTO$_{3-x}$-PVDF||Li pouch cell at 0.5 C at 25 °C.
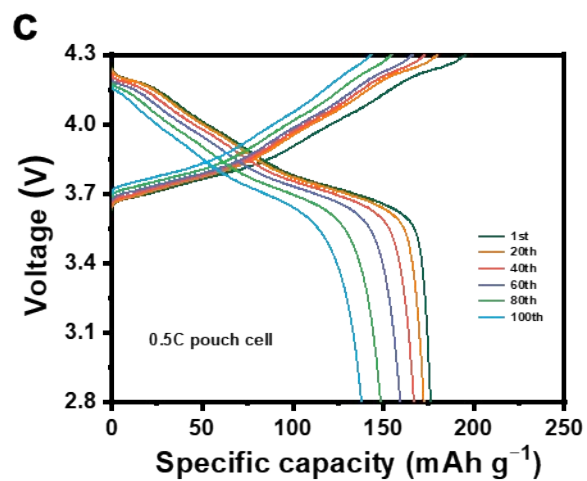
Fig. S31 Charge–discharge voltage profiles of pouch cell at 0.5 C with T-BTO$_{3-x}$-PVDF.
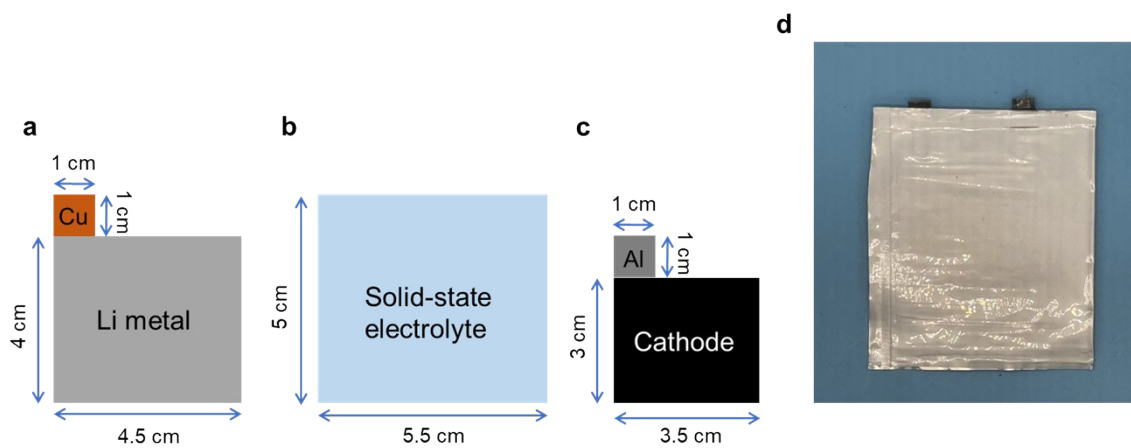
Fig. S32 Schematic diagram of each component of a solid-state pouch battery: a) lithium anode, b) solid-state electrolyte, c) NCM811 cathode. d) pouch battery with T-BTO$_{3-x}$-PVDF electrolyte.
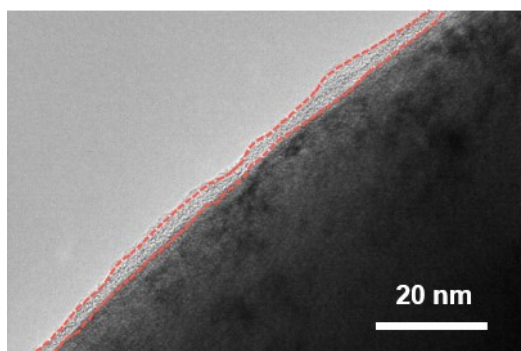
Fig. S33 TEM images of cycled NCM811 particle matching with T-BTO-PVDF.
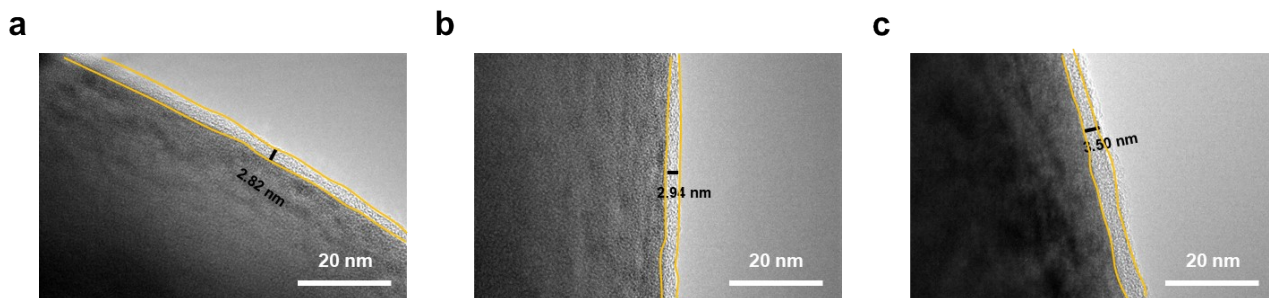
Fig. S34 TEM images of cycled NCM811 particles which are collected in the vicinity of T-BTO.
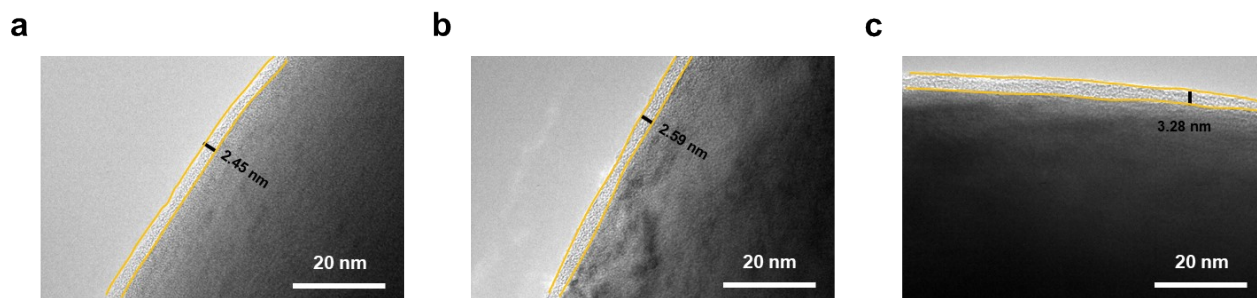
Fig. S35 TEM images of cycled NCM811 particles which are near the current collector.
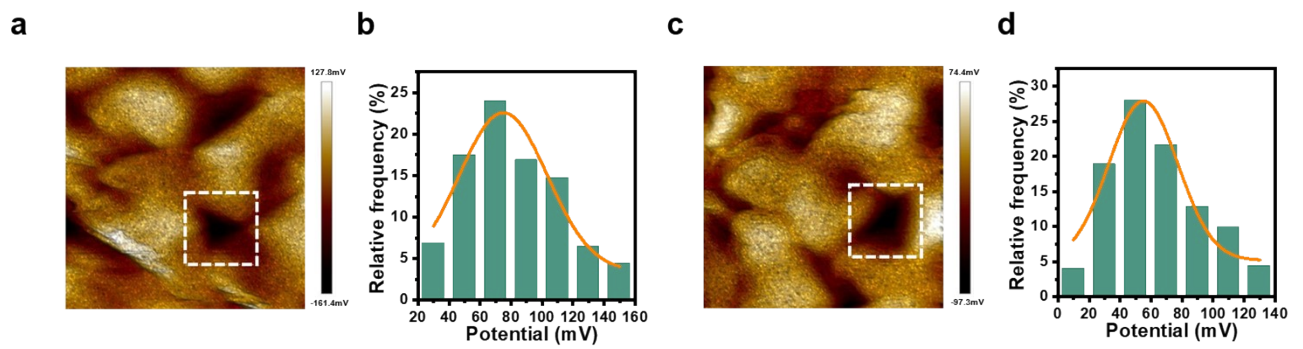
Fig. S36 Kelvin probe force microscopy interfacial potential images of the a) PVDF-NCM811 and c) (T-BTO$_{3-x}$-PVDF)-NCM811. Gauss statistic distribution histograms of the interfacial potential for b) PVDF-NCM811 and d) (T-BTO$_{3-x}$-PVDF)-NCM811.
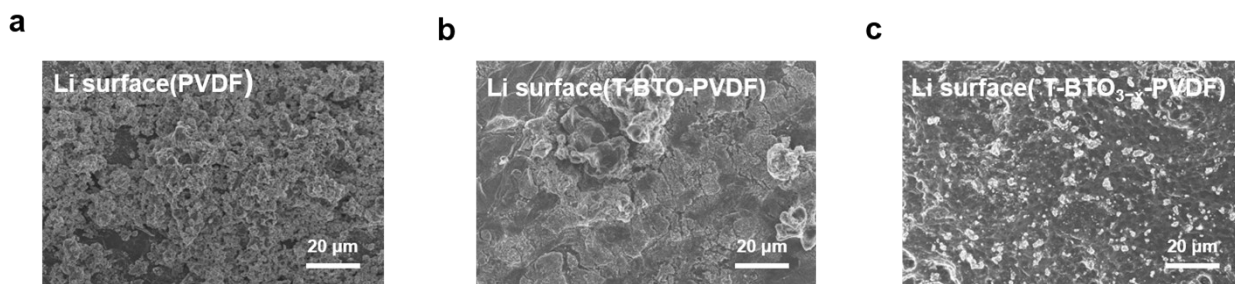
Fig. S37 SEM images of lithium metal surface after cycling 100 h at 0.2 mA cm^{-2} using a) PVDF, b) T-BTO-PVDF and c) T-BTO$_{3-x}$-PVDF.
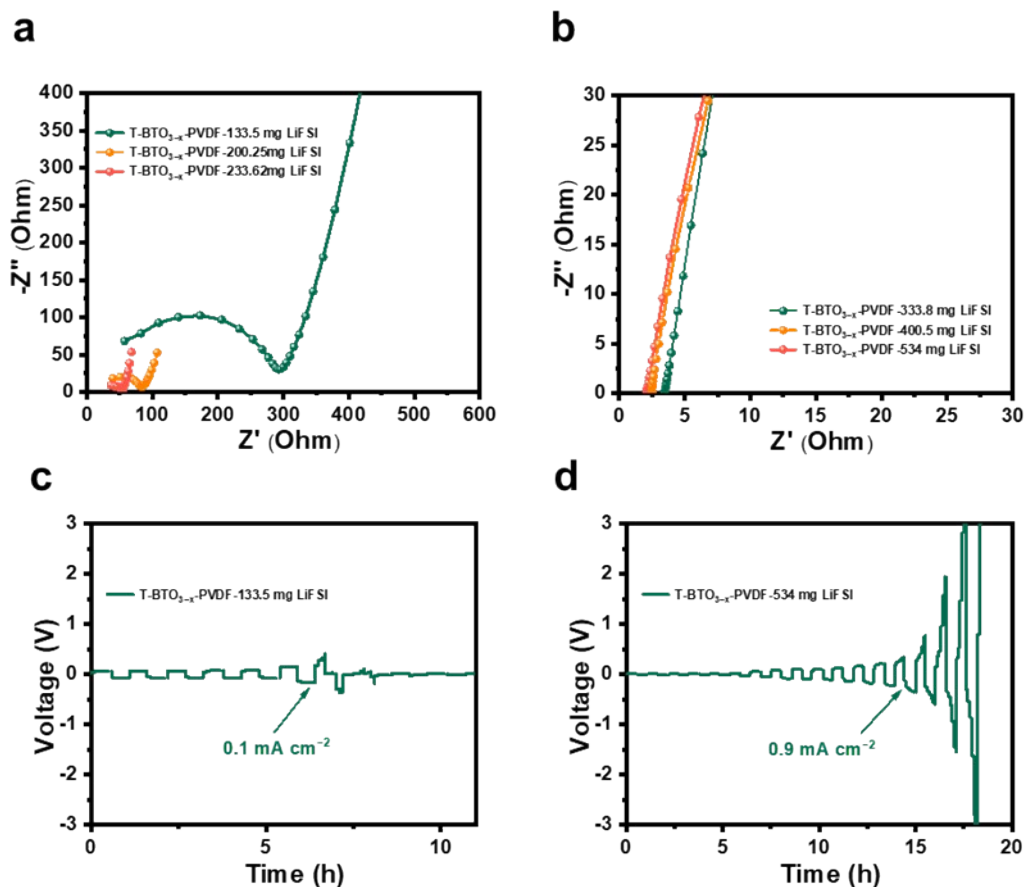
Fig. S38 Influence of lithium salt content on the electrochemical performance of T-BTO$_{3-x}$-PVDF electrolyte. The Nyquist impedance spectra of T-BTO$_{3-x}$-PVDF electrolyte with a) lower lithium salt content and b) higher lithium salt content. CCD of Li∥Li symmetric battery using T-BTO$_{3-x}$-PVDF electrolyte with (c) lower lithium salt content and (d) higher lithium salt content.

Fig. S39 The Nyquist impedance spectra of T-BTO$_{3-x}$-PVDF electrolyte with different filler content.

Table. S1 Transference number and dissociation degree of PVDF-based solid-state electrolytes.

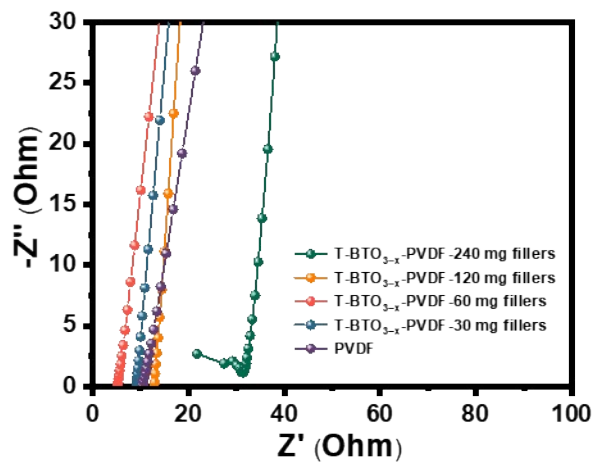| Electrolytes	Transference number	Free Li$^+$	References
PVDF/LiFSI/Coupled BaTiO$_3$-Li$_{0.33}$La$_{0.56}$TiO$_{3-x}$ nanowires	0.57	64%	*Nat. Nanotechnol.*, 2023, 18, 602–610
This work	**0.52**	**72%**	/
PVDF/LiTFSI/100wt% Li$_{6.75}$La$_3$Zr1.75- Ta$_{0.25}$O$_{12}$	0.51	/	*Energy Storage Mater*, 2020, 26, 283-289
PVDF/LiFSI/NaNbO$_3$	0.49	38%	*Adv. Mater*, 2023. 2311195
P(VDF-TrFE-CTFE)/LiTFSI	0.33	/	*Energy Environ. Sci.*, 2021, 14, 6021
PVDF/LiTFSI/8wt% polybenzimidazole	0.49	/	*InfoMat*, 2022, 4, e12247
PVDF/LiFSI/26 wt%/lithium phenyl phosphate	0.47	/	*Energy Environ. Sci.*, 2022, 48, 375-383
PVDF/LiTFSI/15wt% Li$_3$InCl$_6$	0.45	/	*J. Alloys Compd*, 2023, 969, 172418
PVDF/LiTFSI/10%LLZO-10%SN	0.39	/	*ACS Appl. Mater. Interfaces*, 2023, 15, 37422−37432
PVDF/LiTFSI/20wt% PZT	0.37	/	*ACS Nano*, 2023, 17, 14114−14122
PVDF/LiFSI/15wt%LiTaO$_3$	0.33	/	*Energy Mater. Devices*, 2023, 1(1), 9370004

Table S2. The deformation state of PVDF and T-BTO$_{3-x}$-PVDF electrolytes.

	Initial length	Tensile length (stain 30%)	Recovery length	Deformation contribution of Elastic deformation
T-BTO$_{3-x}$-PVDF	10 mm	13 mm	10.46 mm	~85%

Note S1: Preparing samples for ε_r and PFM.

 The testing of ε_r and PFM requires the samples to be free-standing and uniformly thin. Additionally, in order to stimulate the environment in the electrolyte, we selected PVDF without lithium salt as supporting agent. 400mg dry PVDF powders (M_w=300,000, Kynar, 761) without LiFSI was added into 15 ml DMF. Stirring the solution until the PVDF powders were dissolved completely. Then, 15 wt% fillers were added into the solution to slurry 2h and ultrasonic processing 30 min. The obtained solution was poured into petri dish at 55 °C for 30h.

Note S2: Preparing samples for potential between NCM811 and electrolytes.

200 mg dry PVDF powders (M_w=300,000, Kynar, 761) were added into 4.14ml NMP. Stirring the solution until the PVDF powders were dissolved completely. Then, the 30 mg (15 wt% of PVDF) fillers and 800mg NCM811 particles were added into the solution to slurry 5 h. The obtained solution was applied onto the Al foil by a 60 μm scraper. Dry in 80 °C for 1h.